





## Geochemistry, Geophysics, Geosystems

### RESEARCH ARTICLE

10.1029/2017GC007339

# Climatically Driven Changes in the Supply of Terrigenous Sediment to the East China Sea

C. H. Anderson<sup>1</sup> , R. W. Murray<sup>1</sup>, A. G. Dunlea<sup>1,2</sup>, L. Giosan<sup>3</sup>, C. W. Kinsley<sup>4</sup> , D. McGee<sup>4</sup> , and R. Tada<sup>5</sup> 

#### Key Points:

- Multivariate statistical models quantify five East China Sea sediment end-members
- Upper Continental Crust and Luochuan Loess record fluvially supplied Asian material
- Sea level and shelf bypass influenced the amount and composition of terrigenous flux
- Variation in shelf storage may inhibit accurate monsoon reconstructions from fluvial sediment

#### Supporting Information:

- Supporting Information S1
- Table S1

#### Correspondence to:

C. H. Anderson,  
canderso@bu.edu

#### Citation:

Anderson, C. H., Murray, R. W., Dunlea, A. G., Giosan, L., Kinsley, C. W., McGee, D., & Tada, R. (2018). Climatically driven changes in the supply of terrigenous sediment to the East China Sea. *Geochemistry, Geophysics, Geosystems*, 19, 2463–2477. <https://doi.org/10.1029/2017GC007339>

<sup>1</sup>Department of Earth and Environment, Boston University, Boston, MA, USA, <sup>2</sup>Now at Department of Geology and Geophysics, Woods Hole Oceanographic Institution, Woods Hole, MA, USA, <sup>3</sup>Department of Geology & Geophysics, Woods Hole Oceanographic Institution, Woods Hole, MA, USA, <sup>4</sup>Department of Earth, Atmospheric and Planetary Sciences, Massachusetts Institute of Technology, Cambridge, MA, USA, <sup>5</sup>Graduate School of Science, University of Tokyo, Tokyo, Japan

**Abstract** We examine the paleoceanographic record over the last ~400 kyr derived from major, trace, and rare earth elements in bulk sediment from two sites in the East China Sea drilled during Integrated Ocean Drilling Program Expedition 346. We use multivariate statistical partitioning techniques (Q-mode factor analysis, multiple linear regression) to identify and quantify five crustal source components (Upper Continental Crust (UCC), Luochuan Loess, Xiashu Loess, Southern Japanese Islands, Kyushu Volcanics), and model their mass accumulation rates (MARs). UCC (35–79% of terrigenous contribution) and Luochuan Loess (16–55% contribution) are the most abundant end-members through time, while Xiashu Loess, Southern Japanese Islands, and Kyushu Volcanics (1–22% contribution) are the lowest in abundance when present. Cycles in UCC and Luochuan Loess MARs may indicate continental and loess-like material transported by major rivers into the Okinawa Trough. Increases in sea level and grain size proxy (e.g., SiO<sub>2</sub>/Al<sub>2</sub>O<sub>3</sub>) are coincident with increased flux of Southern Japanese Islands, indicating localized sediment supply from Japan. Increases in total terrigenous MAR precede minimum relative sea levels by several thousand years and may indicate remobilization of continental shelf material. Changes in the relative contribution of these end-members are decoupled from total MAR, indicating compositional changes in the sediment are distinct from accumulation rate changes but may be linked to variations in sea level, riverine and eolian fluxes, and shelf-bypass processes over glacial-interglacials, complicating accurate monsoon reconstructions from fluvial dominated sediment.

Received 15 NOV 2017

Accepted 10 MAY 2018

Accepted article online 7 JUN 2018

Published online 11 AUG 2018

## 1. Introduction

The East Asian Monsoon is the dominant climate mode in eastern Asia (Tada, 2004; Wang et al., 2005). At present, the Asian monsoon system influences the development of drought or flooding in some of the most densely populated regions on the globe (Webster et al., 1998). In order to learn about potential climate states of the future, understanding the temporal and spatial variation of past monsoon systems is critical (Nagashima et al., 2013; Tada, 2004). In this context, tracing changes in the terrigenous sediment supply can serve as a useful proxy for monsoonal precipitation and atmospheric regimes during glacial-interglacial periods and during higher-frequency climate variability in East Asia (Clift et al., 2014; Wan et al., 2007).

Hemipelagic sediment of Asian marginal seas records terrigenous material supplied by eolian transport from central Asian deserts and by the major east flowing rivers of the continent (Irinio & Tada, 2000; Wang et al., 2005; Zheng et al., 2013). For example, studies have targeted the sediment export of the Yangtze (Changjiang) River, Yellow (Huanghe) River, and their tributaries during glacial cycles (Dou et al., 2010; Liu et al., 2014; Xu et al., 2012). Weakening of the summer monsoon is likely to have resulted in decreased fluvial transported sediment due to decreased precipitation in southern China (Kubota et al., 2010; Lu & Guo, 2013), but also the potential for increased eolian transport (Hovan et al., 1989). Differences in the geochemical and isotopic composition of fluvial sediment deposited along the continental margins assist in the determination of influence from distinct fluvial drainage basins during different climate conditions through time (Lim et al., 2006; Pisias et al., 2013).

In this study, we aim to reconstruct the temporal variations in provenance and flux of the terrigenous component of East China Sea sediments found at Sites U1428 (31°40.64'N, 129°02.00'E) and U1429 (31°37.04'N, 128°59.85'E) recovered during Integrated Ocean Drilling Program (IODP) Expedition 346. These sediments predominantly reflect fluvial transport from rivers on the Asian continent over the last ~450 kyr (Tada et al., 2013), but also likely include eolian and volcanic aluminosilicate sediment as well. To determine changes in terrigenous provenances through time, we use multivariate statistical techniques applied to an extensive chemical compositional data set generated from bulk sediment chemical analyses. We statistically model East China Sea bulk sediment compositions to identify end-member components, and subsequently discuss the linkages between terrigenous deposition and variability in the East Asian Monsoon system.

## 2. Site Setting, Sample Selection, and Stratigraphy

During IODP Expedition 346, nine sites were drilled in Asian marginal seas and we focus on Sites U1428 (724 m below sea level, [mbsl]) and U1429 (732 mbsl) (Figure 1). These sites are located in the Danjo Basin, at the northern extent of the Okinawa Trough, in the northern East China Sea. At present, these sites lie beneath the Tsushima Warm Current and are influenced by the summer expansion of East China Sea Coastal Water from increased Yangtze River discharge (Gallagher et al., 2015). At both of these sites, the sedimentation rates are very high, averaging 43 and 51 cm/kyr at U1428 and U1429, respectively. Although Sites U1428 and U1429 are currently ~700 km from the Yangtze River, these sites were likely located ~400 km northeast of the advancing Yangtze River mouth, and as close as ~150 km from the Yellow River mouth during glacial sea level lowstands (Uehara et al., 2002). Thus, these sites are ideal to reconstruct East Asian Monsoon precipitation and river transport of fine-grained continental detrital material (Kubota et al., 2010).

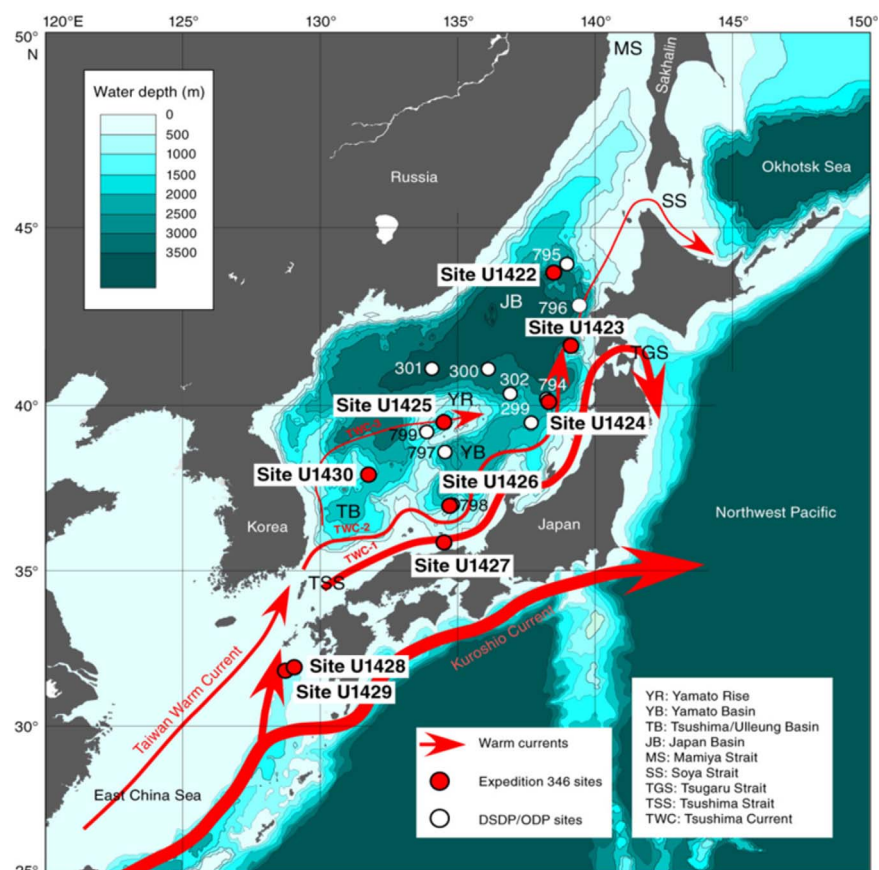


**Figure 1.** Bathymetric map of sites from IODP Expedition 346 (red circles), previous DSDP/ODP drill sites (white circles), and present surface currents (red arrows). From Tada et al. (2013).

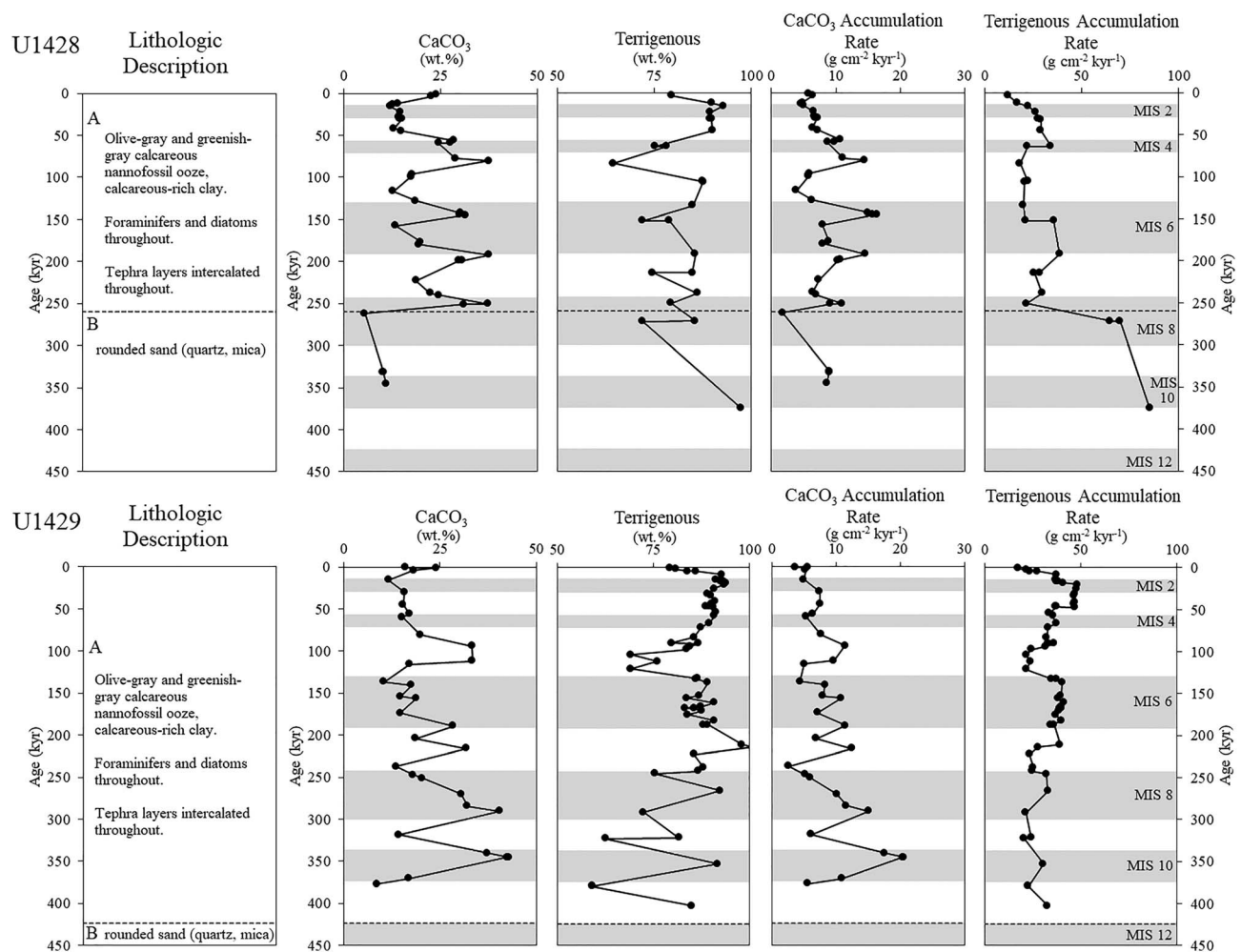


**Figure 2.** Shipboard lithologic summaries,  $\text{CaCO}_3$  content (wt. %), Terrigenous content (wt. %),  $\text{CaCO}_3$  accumulation rate ( $\text{g cm}^{-2} \text{ kyr}^{-1}$ ), and terrigenous accumulation rate ( $\text{g cm}^{-2} \text{ kyr}^{-1}$ ) are plotted with age (kyr) at IODP Sites U1428 (top) and U1429 (bottom). Ages were determined from the benthic oxygen and tephrostratigraphic age model from Sagawa et al., (2017). Horizontal shaded regions indicate glacial periods (Lisiecki & Raymo, 2005). Accumulation rates are calculated from dry bulk density, linear sedimentation rate, and the resulting bulk accumulation rate.  $\text{CaCO}_3$  accumulation rate was calculated from the shipboard  $\text{CaCO}_3$  concentration data (Expedition 346 Scientists, 2014) and interpolated bulk accumulation rate. These calculations and parameters are discussed in the supporting information.

The sediment at these two sites is divided into two lithologic units defined by calcareous nannofossil ooze, calcareous-rich clays interbedded with tephra layers (Unit A) and a second unit of rounded, fine-grained sands (Unit B) (Figure 2). Numerous tephra layers, ranging from decimeters to half meters, occur throughout (Tada et al., 2013). It is also possible that very fine-grained turbidites in this record were not visible in core description, as will be apparent in later geochemical discussions. The sands of Unit B prevented recovery of materials deeper than 200 m below seafloor (mbsf) at Site U1428, as these sand beds extended through the bottom 37 m of the total core recovery. Site U1429 (188 m of recovered core) was drilled in an attempt to recover Miocene-aged sediment, but the sands of Unit B were also present at this location. There is minimal opal at these sites, as the biogenic component primarily consists of  $\text{CaCO}_3$  (Figure 2) with concentrations ranging between 15 and 40 weight % (wt. %) (Expedition 346 Scientists, 2014). While a portion of the total  $\text{CaCO}_3$  may be detrital and missed by sedimentologists during core description, the lithostratigraphic descriptions, including smear slides analysis, indicates local biogenic sources from the overlying ocean. The redox state of the sediment is modestly reducing (Calvert & Pedersen, 1993; Morford & Emerson, 1999) and does not compromise the ability of the sedimentary chemistry to facilitate provenance determination (supporting information). Additional important information about the sedimentology and stratigraphy, including age models, of these sites is provided in supporting information.

### 3. Geochemical Analytical and Multivariate Statistical Methods

#### 3.1. Samples and Geochemical Analytical Methods

A total of 82 bulk sediment samples from Unit A at Sites U1428 and U1429 were used for this work. Fifty-two of these samples were collected at the time of coring and are evenly spaced, bulk sediment samples consisting of 5 cm-long whole-round samples that were squeezed for shipboard pore water analysis and discrete 2 cm plug samples collected for shipboard analysis of carbonate abundance. An additional 30 discrete samples were collected during shore-based sampling to fill in temporal gaps in the first sampling prior to the development of the age model. Details regarding the geochemical sample preparation, including a discussion of how analytical precision and accuracy were quantified (Ireland et al., 2014), are found in supporting information.

#### 3.2. Multivariate Statistical Methods

The geochemical data set was analyzed using multivariate statistical MATLAB™ algorithms from Piasias et al. (2013) and Dunlea and Murray (2015). We take a multistep statistical approach optimized for sediment geochemistry that uses Q-mode Factor Analysis (QFA) and Constrained Least Squares multiple linear regression (CLS). The implementation and interpretation of these techniques are guided by element ratio downcore profiles and ternary plots to ensure the statistical results are consistent with the basic characteristics of the data set. These techniques have been used in a variety of marine settings by our research group (Dunlea et al., 2015; Martinez et al., 2009; Scudder et al., 2016; Ziegler et al., 2007 and references therein).

We use QFA to determine the minimum number of components necessary to explain a given fraction of total variance in a data set by identifying groups of covarying elements into “factors” (Piasias et al., 2013). Factors are then VARIMAX rotated to maintain orthogonal relationships while maximizing the variance explained by each factor. The approach is based on the assumptions that unique sediment sources are represented by each VARIMAX-rotated factor, and that the elements included in each factor are basic indications of that factor’s representation of sediment source. The strength of element covariance is indicated by high absolute factor scores, and the importance of each factor to the variability in a given sample by the factor loading value. This loading value indicates variation in the importance of a factor throughout the data set, which in our case means through a sediment column and thus through time.

Following QFA, we build on the number and general characteristics of the bulk sediment factors, and apply an iterative algorithm for CLS multiple linear regression models to identify and quantify the proportion of each end-member in each discrete sample (Dunlea & Murray, 2015; Piasias et al., 2013). The CLS code creates multidimensional mixing models that minimize the sum of the squared statistical residuals between the model and the sample data set, while optimizing the proportions of each end-member in each sample. The number of QFA identified factors correspond to the total number of end-members to be modeled in CLS iterations. A collection of geologically reasonable source rock geochemical compositions from a range of literature and reference materials were compiled to serve as the potential end-member inputs that correspond to the QFA defined factors. This collection was developed based on the QFA results as well as characterization from the literature of the paleoceanographic and geological systems under investigation. As detailed in section 4.3, we used a preliminary geochemical set including different types of continental crust components, Chinese loess, paleosols, and mafic sources (e.g., basalts, tephra, tuffs) to constrain the “families” of potential end-member sources for CLS modeling.

Multiple tests were conducted to check the statistical stability of the modeling and to ensure that the identification and composition of the factors are not overly sensitive to the statistical parameterizations, including minor changes in the chemical element menu. Factors were accepted that explained greater than 2% of variance in the data set to avoid insignificant factors related to analytical precision (Additional discussion of QFA factor selection is in the supporting information). Additional model iterations were conducted to determine if the greater number of samples from Site U1429 influenced the resulting factors when both sites were combined into a single data set. For this, 24 samples at approximately equal depth spacing were selected to ensure that factors identified during iterations with the reduced data set were in agreement with iterations utilizing the full data set.

#### 4. Geochemical Trends

Downhole geochemical profiles indicate that sediment at Sites U1428 and U1429 are a complex mixture of multiple aluminosilicates in a reducing environment. In this section, we explore the downhole geochemical trends through a first-order assessment of the bulk sediment using a variety of traditional graphical partitioning techniques applied to geochemical compositions. This knowledge is then used to guide the QFA and CLS multivariate statistical techniques that focus on provenance, as discussed in section 5.

During these geochemical explorations, we use a collection of well-constrained crustal compositions as reference values. We use post-Archean Australian Shale (PAAS), Upper Continental Crust (UCC), Mid Ocean Ridge Basalt (MORB), and Chinese Loess (CL) as reference compositions, and *only* as reference compositions (Gale et al., 2013; Taylor & McLennan, 1985). Although geochemically discrete, we do not interpret the potential compositional similarities of the bulk sediment geochemistry at Sites U1428 and U1429 to these reference materials to require that the ultimate sediment composition is directly tied to these geographic source areas (e.g., post-Archean Australian Shale) or to prescribe a transport pathway implied in the name of the material (e.g., eolian transport of “Chinese Loess”).

The downhole profiles indicate periods of mixing between continental reference compositions similar to those represented by PAAS, UCC, and CL (Figure 3). The geochemical trends at these sites also are not in concert with changes in the bulk accumulation rates (Figure 2). The majority of the downhole profiles generally indicate mixing between PAAS and CL-type compositions, along with suggestions of mixing between PAAS-like and MORB-like (e.g., Rb/Al), or between CL and UCC-like (e.g., Cr/Al).

However, there are notable excursions downhole between these sources that are similar to the reference compositions and downhole elemental ratio profiles, and other graphical techniques also do not clearly untangle the potential sources and the mixing history. For example, from 70 to 80 kyr the profiles of Rb/Al, La/Al, and Th/Al suggest the presence of a mafic MORB-like component, yet Ti/Al suggests UCC mixing. There is another decrease in various elemental ratios in downhole profiles between ~ 210 and 240 kyr, which may suggest the presence of both UCC-like and MORB-like components, while PAAS-like and CL-like compositions are also within the mixing field, indicating the complexity in the system outside of simplified two-component mixing through time. Site U1428 also requires additional partitioning techniques to sufficiently describe mixing.

Contrasting patterns in ternary diagrams further highlight the complexities of determining mixing. Robust mixing lines for both sites between continental crust values (UCC, multiple loess compositions) and more mafic end-members (Japanese Andesite, MORB) in the La-Th-Sc diagram highlight the small geochemical variability of the samples (Figure 4). Other combinations (e.g., Rb-Th-Cr) exhibit two arrays offset in compositional space, indicating multiple mixing relationships.

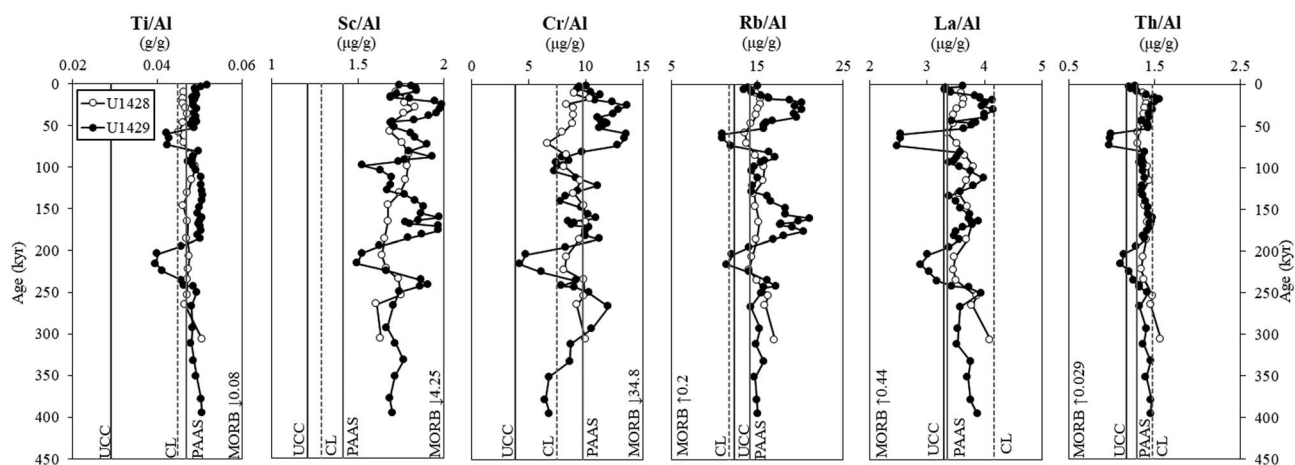


**Figure 3.** Element ratio (g/g and  $\mu\text{g/g}$ ) age profiles for both sites. Shown for reference, the gray vertical lines depict average values for upper continental crust (UCC), Chinese Loess (CL), post-Archean Australian average shale (PAAS) (Taylor & McLennan, 1985), and mid ocean ridge basalt (MORB) (Gale et al., 2013).

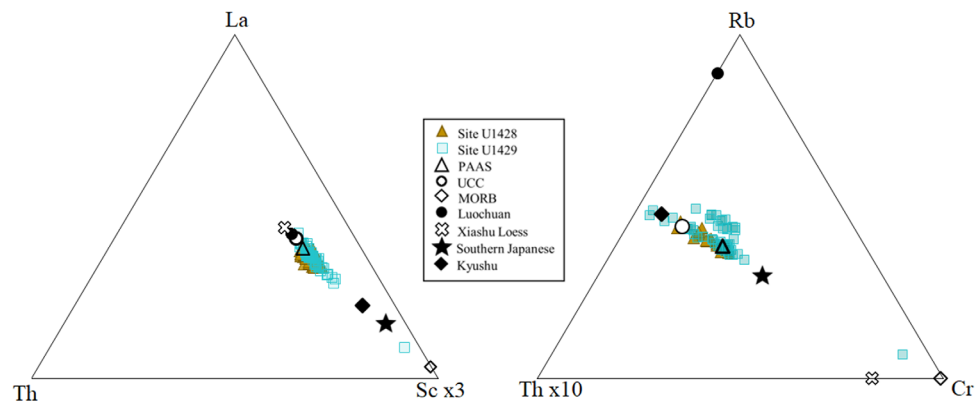


**Figure 4.** Bulk sediment samples plotted on ternary diagrams with end-member compositions. La-Th-Sc diagram indicates mixing between mafic and felsic end-members. Rb-Th-Cr indicates two mixing arrays that skew toward Th, respectively.

Although none of the downhole profiles of major sedimentary components (Figure 2), elemental ratios (Figure 3), or ternary diagrams (Figure 4) clearly indicate a unique set of terrigenous sources to Sites U1428 and U1429, examination of these figures collectively indicates:

1. Despite being a low-resolution record, the concentration of  $\text{CaCO}_3$  (wt. %) from the shipboard data appears to decrease during glacial periods. The pattern of  $\text{CaCO}_3$  accumulation rate shows the same general pattern, indicating that changes in  $\text{CaCO}_3$  concentration are not solely due to terrigenous dilution.
2. There is no clear relationship between variability in the terrigenous elemental ratios and bulk accumulation rate, indicating compositional changes are decoupled from accumulation rate changes.

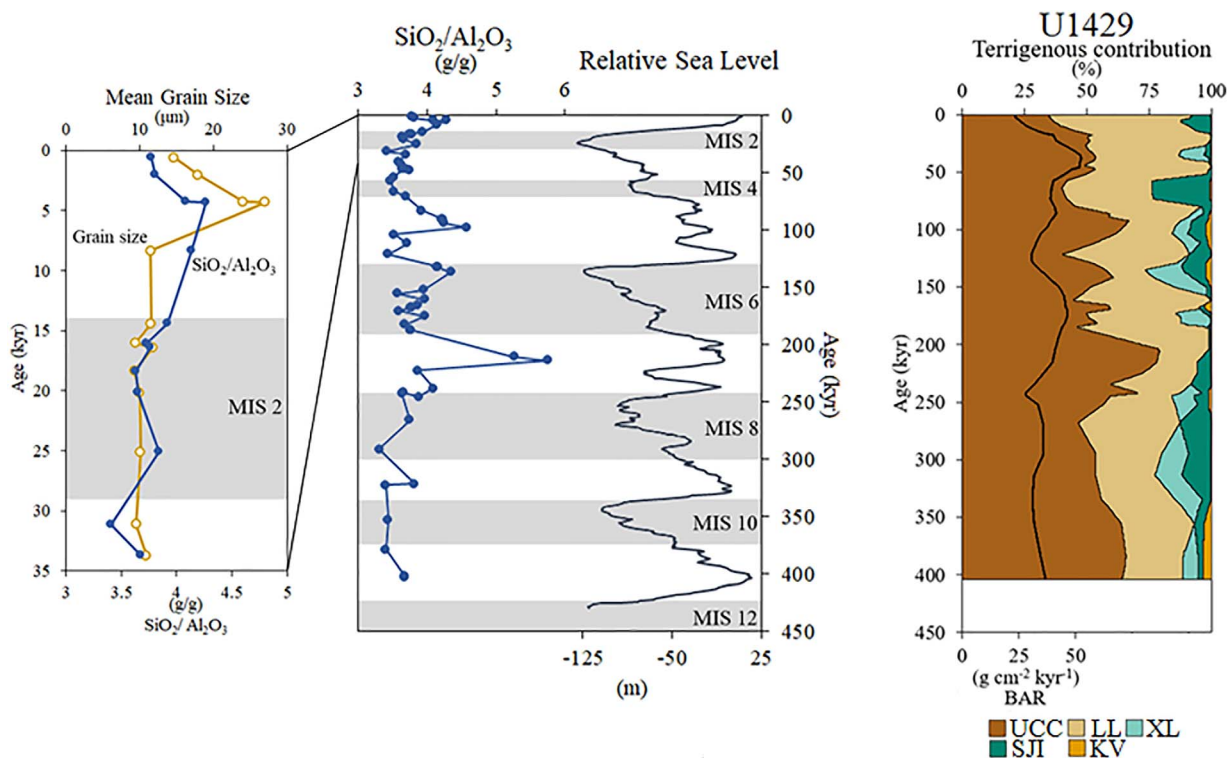


**Figure 5.** (left) Grain size proxy  $\text{SiO}_2/\text{Al}_2\text{O}_3$  ratio (g/g, blue line with closed circles) presented with relative sea level (black line) (Spratt & Lisiecki, 2016) over the last 450 kyr. Mean grain size ( $\mu\text{m}$ ) from Zhao et al. (2017) (yellow line with open circles) and  $\text{SiO}_2/\text{Al}_2\text{O}_3$  are compared over the last 34 kyr. The y-axis is age (kyr) and horizontal shaded regions indicate glacial periods (Lisiecki & Raymo, 2005). (right) Comparison of Bulk Accumulation Rate (BAR,  $\text{g cm}^{-2} \text{ kyr}^{-1}$ ) and terrigenous contribution (%). BAR is plotted as the solid black line. The end-member contributions are plotted to sum to 100%, with each color representing the sum of each end-member contribution plus the end-members to the left. The total terrigenous fraction is dominated by the UCC-like end-member.

3. There are some consistent patterns with depth and in ternary space, but mixing solutions are ambiguous without additional investigation.

## 5. Provenance Assessment

Site U1428 records the broad trends in terrigenous accumulation (supporting information), so we focus on the longer, higher-resolution record from Site U1429 in the following sections. We gathered more samples from Site U1429 ( $n = 58$ ) compared to Site U1428 ( $n = 23$ ), so the statistical results are more robust at Site U1429. In the subsequent statistical modeling, a consistent suite of elements was utilized. The refractory elements selected for the provenance menu (Al, Ti, Sc, Cr, Rb, Th, and La) are not diagenetically reactive (Taylor & McLennan, 1985), are commonly associated with different crustal components, and therefore have been used in many previous provenance studies (Dunlea et al., 2015, and references therein).

QFA based on this refractory element menu resulted in five significant terrigenous factors that explain 99% of the variance of the data set. The results from the QFA are expanded upon in the supporting information. The total number of factors determined from the QFA were used to inform the subsequent CLS multiple linear regressions. We first identified 23 potential end-members from the GEOROC database (supporting information) that could fit the broad requirements indicated by the QFA. Then, using the CLS codes of Dunlea and Murray (2015), tens of thousands of combinations involving 23 geologically probable end-member compositions were tested (Table 1). We used possible end-members of varying composition including aluminosilicate upper continental sources (e.g., PAAS, UCC, Chinese Upper Continental Crust, multiple Chinese loess sources from the loess plateau and major river drainage basins, and crustal components from Southern Japanese Islands), and more mafic sources (e.g., MORB, andesites, and certain appropriate Japanese volcanics including from the local Kyushu volcanoes Aira, Aso, and Ata). Goodness-of-fit parameters were recorded for each CLS model iteration and the models that had the highest coefficients of determination were identified (supporting information). This process of using every combination of five end-members

**Table 1**

References for Each End-Member are Listed in the Last Column

End-member	Al (wt. %)	Ti (wt. %)	Sc (ppm)	Cr (ppm)	Rb (ppm)	Th (ppm)	La (ppm)	Reference
Post-Archean Australian Average Shale (PAAS)	10.00	0.60	16.00	110.00	160.00	14.60	38.00	Taylor and McLennan (1985)
Upper Continental Crust (UCC)	8.04	0.30	11.00	35.00	112.00	10.70	30	Taylor and McLennan (1985)
Mid-Ocean Ridge Basalt (MORB)	7.78	1.01	39.80	249.00	2.88	0.40	5.21	Gale et al. (2013)
Chinese Loess (CL)	6.72	0.41	11.90	69.00	108.00	9.89	28.49	Taylor and McLennan (1985)
Luochuan Loess	6.48	0.40	10.84	70.60	93.98	12.36	33.15	Gallet et al. (1996); Chen et al. (1996)
Xiashu Loess	7.45	0.54	13.90	88.49	119.00	16.46	44.40	Chen et al. (2008); Hao et al. (2010)
Chinese Upper Crust	7.25	0.40	16.67	89.33	84.67	9.68	33.88	Gao et al. (1998)
Chinese Total Crust	7.22	0.42	16.67	86.67	71.33	7.80	32.48	Gao et al. (1998)
Kyushu <sup>a</sup>	8.34	0.79	26.93	86.67	62.47	6.07	22.01	GeoRoc
Kyushu and surrounding islands <sup>a</sup>	8.52	1.15	26.59	94.90	55.43	5.48	22.26	GeoRoc
Kyushu Volcanics <sup>a,b</sup>	8.04	1.31	30.21	69.67	80.01	7.46	24.68	GeoRoc
Southern Honshu <sup>a</sup>	8.07	0.62	16.34	82.27	70.42	8.40	36.27	GeoRoc
Southern Japanese Islands <sup>a</sup>	8.69	0.44	27.45	43.17	46.01	3.88	13.15	GeoRoc
Ryukyu Arc <sup>a</sup>	9.01	0.45	34.20	37.25	46.07	2.97	8.19	GeoRoc
Shikoku <sup>a</sup>	8.07	1.00	26.68	111.42	54.00	8.74	24.73	GeoRoc
Yufu-Tsurumi <sup>a</sup>	8.81	0.68	126.34	32.18	38.92	5.05	14.76	GeoRoc
Aso <sup>a</sup>	8.81	0.45	12.30	9.59	125.95	13.96	31.23	GeoRoc
Aira <sup>a</sup>	8.16	0.41	19.00	117.00	44.49	4.61	13.88	GeoRoc
Hiradoshima <sup>a</sup>	8.70	0.65	26.70	258.93	48.05	4.73	23.53	GeoRoc
Itsuki Island <sup>a</sup>	9.29	1.03	23.44	149.41	45.06	5.70	37.44	GeoRoc
Kaimon-dake <sup>a</sup>	9.49	0.67	28.80	10.00	17.90	1.89	11.10	GeoRoc
Okue-yama <sup>a</sup>	7.73	0.34	10.35	11.00	166.83	12.90	36.95	GeoRoc
Ontake <sup>a</sup>	7.20	0.14	3.76	1.60	116.00	10.82	27.08	GeoRoc

<sup>a</sup>End-members are average compositions of whole rocks or <sup>b</sup>volcanic material from various Japanese islands downloaded from GEOROC database accessed January 2017 (<http://georoc.mpch-mainz.gwdg.de/georoc/>). Prior to averaging GEOROC data, extreme outliers were removed. End-member compositions are over specified to minimize artifacts from rounding.

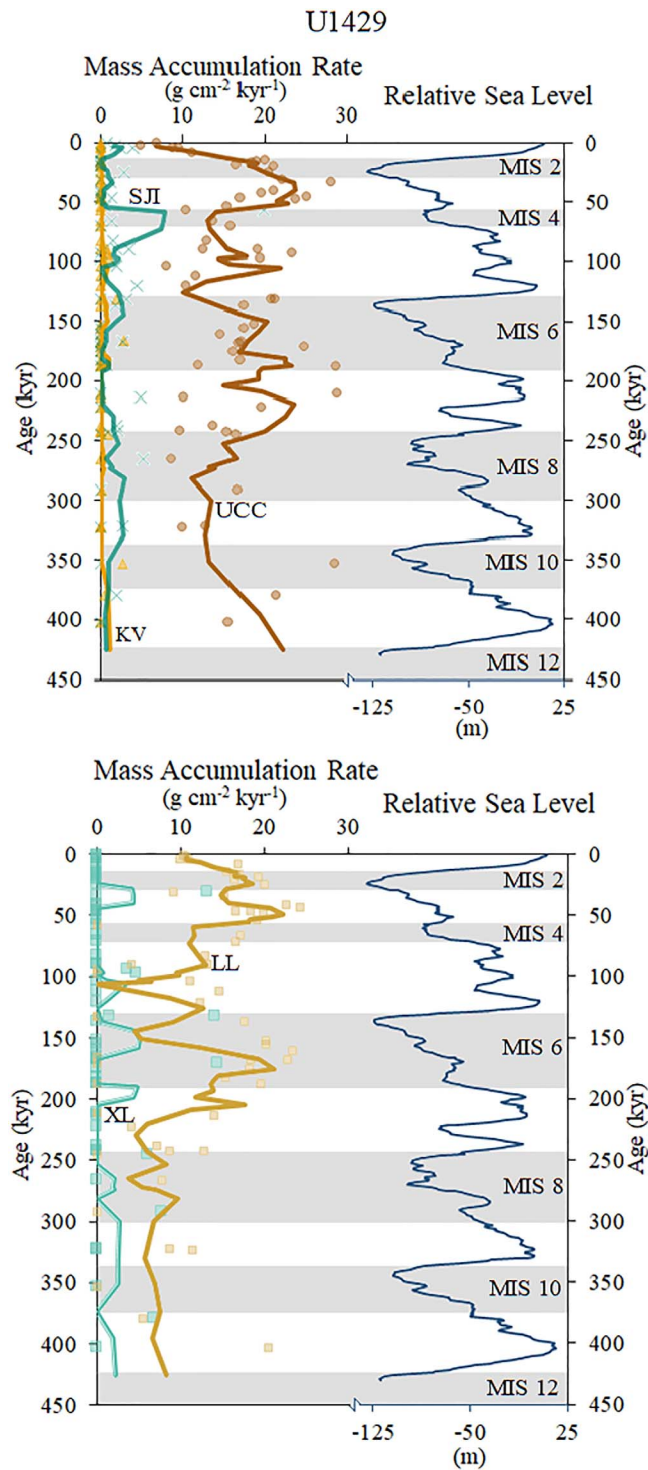


**Figure 6.** Mass accumulation rates (MAR) of five end-members produced by the CLS models of terrigenous sediment provenance (UCC: Upper Continental Crust, LL: Luochuan Loess, XL: Xiashu Loess, SJ: Southern Japanese Islands, KV: Kyushu Volcanics). End-member MARs are plotted as 3 point moving averages (lines) and discrete sample accumulation rates (points). Relative sea level (blue line) and glacial Marine isotopic stages (MIS) (shaded regions) are plotted for reference (Spratt & Lisiecki, 2016).



from this extensive list to identify the combination(s) that best fits the data allows the identification of the most probable compositional end-members contributing to the bulk sediment.

Iterations resulted in several hundreds of potential CLS models. From the top 300 models, the best were ranked, and subsequently selected, based on the highest sum of coefficients of determination. This selection process is described more fully in the supporting information. From the top ~10 CLS models that best fit the data set, the end-members were consistently UCC, Luochuan Loess, Xiashu Loess, and composite end-members Kyushu Volcanics and Southern Japanese Islands (see supporting information). In the below sections, the presence and significance of these sources are discussed.

### 5.1. Upper Continental Crust End-Member

Including generic Upper Continental Crust (UCC) in the end-member menu consistently produced model outcomes with the highest goodness-of-fit and that explain 99% of the data set. This is geologically reasonable due to the nearby position of Asia and potential fluvial erosion, and that this generic composition itself is a compilation in its own right (Taylor et al., 1983). The inclusion of loess-like compositions in the construction of the UCC composite may complicate the ultimate determination of transport mechanisms (e.g., fluvial versus eolian), however the models require that we use this end-member for the most robust results. Throughout this record, UCC consistently contributes between 35 and 79% of the total terrigenous fraction. The local maxima (or “peaks”) in UCC contribution (weight %) occur between 18 and 45 kyr, 85 and 105 kyr, 130 and 150 kyr, 195 and 240 kyr, and 290 kyr to the end of the record at 400 kyr (Figure 5).

The UCC mass accumulation rate exhibits several local maxima between 18 kyr and 45 kyr, 85 and 95 kyr, 125 and 140 kyr, 160 and 168 kyr, 195 and 218 kyr, with an absolute maximum accumulation rate of 24 g/cm<sup>2</sup>/kyr at 35 kyr. During the majority of this record, UCC mass accumulation rates typically ranges between 7 and 20 g/cm<sup>2</sup>/kyr (Figure 6).

### 5.2. Chinese Loess End-Members

Two different Chinese loess end-members were consistently in the models with the highest goodness-of-fit parameters. The average compositional value from the well-characterized Luochuan Loess sequence was consistently a statistically optimal end-member in the best fit models. In this model, Luochuan Loess may represent a loess value from the Chinese Loess Plateau. Xiashu Loess, an epigenetic loess sequence from the Yangtze River drainage basin enriched in Fe, Ti, and certain trace elements (e.g., Th, Zn, Ni, Cr, V) (Chen et al., 2008; Gong et al., 1987) was also consistently a second loess end-member in the best fit models. The inclusion of these two loess end-members does not necessarily imply a transport mechanism (e.g., eolian); they are solely used for the ability of their chemical composition to explain statistical variability in the data set. For example, material from terrestrial loess deposits in the Asian interior could be transported by rivers, remobilized from the continental shelf, or indeed carried by winds prior to deposition at the locations of Sites U1428 and U1429, or, of course, by combinations of these transport mechanisms. As will be addressed in later sections, true eolian transported inputs are minimal and are not important relative to the significant fluvial input. Regardless, these two loess compositions, sourced from different locations in the Asian interior, are a strong, required presence in robust model outcomes.

The loess end-member contributions and mass accumulation rates exhibit variation over time. Luochuan Loess contributes between 16 and 55% of the terrigenous fraction throughout this record, while Xiashu Loess contributes 4–15% *when present*. Peaks in Luochuan Loess abundance in the bulk sediment occur from present until 8 kyr, 16–25 kyr, 40–55 kyr, 70 kyr, 110 kyr, 135–160 kyr, and 185 kyr, with a general increase in contribution from 16 to 25% contribution from 210 kyr until the end of the record (Figure 5). There are several periods of gradually increasing Luochuan Loess accumulation between approximately 18–45 kyr and 150–185 kyr, with the maximum accumulation rates of 22 g/cm<sup>2</sup>/kyr occurring at approximately 43 kyr and 155 kyr (Figure 6). The Xiashu Loess end-member is also variable over time, but exhibits a smaller relative contribution than the Luochuan end-member.

When present, Xiashu Loess contributes to the terrigenous fraction between 25 and 35 kyr, 90 and 100 kyr, 125 and 140 kyr, 165 and 175 kyr, 235 and 245 kyr, and 290 kyr to the end of the record (Figure 5). There are several local maxima of the Xiashu Loess accumulation rate from approximately 30–35 kyr, 100–105 kyr, 130–145 kyr, and 175–180 kyr. Xiashu Loess reaches its maximum accumulation rate of 5 g/cm<sup>2</sup>/kyr at approximately 140 kyr (Figure 6).

### 5.3. Southern Japanese Island and Kyushu Volcanic End-Members

The CLS models with the highest goodness-of-fit also used combined end-members of Southern Japanese Islands and Kyushu Volcanics. Again, this is consistent with the geological and geographic environment, given the proximity of the Japan Arc. "Southern Japanese Islands" is a compilation of more felsic, granitic crustal values from Kyushu, Shikoku, and other islands in the Ryukyu Arc, while Kyushu Volcanics is a compilation of volcanic lavas, ashes, and basalts sourced from Kyushu. Included in this end-member are several tephra used in tephra chronology, including several Aso, Aira, and Ata tephra (Ikehara, 2015). Both of these end-members exhibited low concentrations through time, but are necessary requirements to model the variability of the data set.

The source from the Southern Japanese Islands ranges between 1 and 23% of the terrigenous contribution, while the Kyushu Volcanics range between 1 and 3% when present. Southern Japanese Islands input is found from the present to 4 kyr, 18–30 kyr, 48–85 kyr, 100–135 kyr, 160–167 kyr, and 185 kyr until the end of the record. Local maxima in Southern Japanese Islands contribution occur between 5 and 10 kyr, 50 and 75 kyr, 115 and 140 kyr, and 250 and 293 kyr (Figure 5). The mass accumulation rate of the Southern Japanese Islands end-member increases between 55 and 75 kyr, 130 and 140 kyr, reaching a maximum accumulation rate of 7 g/cm<sup>2</sup>/kyr at 65 kyr (Figure 6), from a background of approximately 2 g/cm<sup>2</sup>/kyr. Pulses in the mass accumulation rate of this end-member help explain the depletions toward general crustal values seen in the Ti/Al ratios (Figure 3).

The Kyushu Volcanics end-member appears in the record several times. This end-member contributes to the terrigenous fraction between 85 and 100 kyr, 110 and 130 kyr, 155 and 165 kyr, 222 and 245 kyr, and 260 kyr to the end of the record. The Kyushu Volcanics end-member accumulation rate was consistently less than 1 g/cm<sup>2</sup>/kyr through time, but is necessary to constrain the general enrichment in Ti/Al towards mafic compositions through the record (Figure 3).

The total terrigenous fluxes are not directly linked to the same end-members through time, as Southern Japanese Islands and Kyushu Volcanic end-members have a higher mass accumulation rate even at times of lower total terrigenous accumulation rate. Southern Japanese Islands may represent fluvially transported crustal material from several southern islands in the Japanese archipelago and therefore reflect changes in local/regional sediment supply. The Kyushu Volcanics end-member may represent a combination of airborne ashes, or fluvially transported volcanic material from the Japanese archipelago, separate from processes on the Asian continent. Specifically, the Kyushu Volcanics end-member may trace activity of the Aso Volcano on Kyushu, as the chemically and temporally well-characterized tephra Aso-1, Aso-3, and Aso-4 are included in this end-member (Ikehara, 2015). Accumulation peaks in this end-member occur approximately at the same time as these tephra deposits, and may also represent discrete and dispersed ash.

## 6. Geochemical Evolution of the East China Sea

There are multiple sources contributing terrigenous aluminosilicate material to the bulk sediment at Sites U1428 and U1429. All five components are broadly similar in that they include upper continental crustal composition(s), loess, and ash, and we reinforce that having the five distinct components is required by both the QFA approach and the CLS linear regressions. We further emphasize that, even though some of the end-member compositions are best approximated by loess compositions, such a determination does not require an eolian pathway by which that loess composition arrives on the seafloor at Sites U1428 and 1429. Specifically, our approach alone cannot definitively differentiate direct deposition of eolian dust from the fluvial transport of eroded terrestrial loess deposits.

Nonetheless, there are a number of different mechanisms that potentially could explain the changes through time in the composition of the terrigenous component(s) as well as the flux(es) of the different component(s). These include variability in the (1) strength and/or position of the Kuroshio Current, (2) proportion of sediment supply from fluvial or eolian transport, or (3) shelf bypass processes, as discussed below. Examining the changes in source composition, and the changes in absolute and relative fluxes, helps to shed light on the climatically controlled inputs of terrigenous material to the East China Sea and potential complications in climate reconstructions from fluvial-dominated sediment.

### 6.1. Changes in Path and Intensity of the Kuroshio Current

We first consider the potential influence of changes in the Kuroshio Current to the sediment record at these sites. There is limited agreement as to the path and intensity of the Kuroshio during glacial/interglacial sea level change. Models either indicate deflection of the boundary current eastward of the Ryukyu Arc (Ujiié & Ujiié, 1999), or suggest that the Kuroshio maintained a path through the ECS and along the shelf-break (Dou et al., 2010). Paleoceanographic proxies suggest that the path of the Kuroshio followed the shelf-break on the eastern edge of the Okinawa trough during glacial lowstands (Gallagher et al., 2015; Kawahata et al., 2006; Lee et al., 2013), which may have limited shelf-bypass of sediment and deposition in deeper settings east of the Okinawa Trough and continental shelf.

These Kuroshio processes may have contributed to changes in deposition at Sites U1428 and U1429, but cannot be uniquely isolated with our current data set. Nonetheless, as will be seen in the following discussions, we can explain the sedimentary record at these sites entirely considering only erosional, eolian, and/or sea-level related depositional processes. While we cannot exclude that there are paired impacts from changes in strength or location of the Kuroshio that are occurring simultaneously with these other climate-related processes, there is no requirement to invoke such Kuroshio-related changes to explain the sedimentary chemical record at Sites U1428 and U1429. Ongoing high-resolution scanning XRF studies of these same sites may add to this discussion in the future.

### 6.2. Differentiating Fluvial and Eolian Transport

In this region, it is expected that dust fluxes would increase during glacial periods as vegetation in northern China is more sparse, and the frequency of high-speed wind events and wind intensity may increase (McGee et al., 2010; Nagashima et al., 2007). This is a difficult process to untangle, however, since much of the terrigenous sediment that would be transported by wind is compositionally similar to material that would be transported by rivers from the Asian interior, or transported through terrestrial eolian deposition and remobilization, and possible fluvial reworking, before ultimate deposition in the ocean.

The most conservative interpretation is to consider that the generic UCC end-member, which contributes more than 50 weight % of the terrigenous fraction, represents the primary fluvial component of terrestrial material transported by the major Asian rivers that are, after all, quite nearby and are very large. Additionally, the increase in dust deposition to the Asian interior may also influence sediment composition transported through the fluvial pathway. Increased dust deposition on the Chinese Loess Plateau may supply loess-like material to the river systems, shifting the fluvial signal from UCC-like composition to more loess-like.

For example, Zhao et al., (2017) identified a Yellow River end-member in the clay fraction of the sediment at site U1429. This Yellow River end-member has an average LGM accumulation rate of 35.7 g/cm<sup>2</sup>/kyr, and 11.2 g/cm<sup>2</sup>/kyr during the Holocene. In our models, UCC accumulation rate during the LGM is 18 g/cm<sup>2</sup>/kyr, and the accumulation rate of Luochuan Loess is 17 g/cm<sup>2</sup>/kyr. If we assume that both of these end-members are transported by rivers and/or as the result of reworked loess in the Yellow River drainage basin, our model estimate of accumulation (35 g/cm<sup>2</sup>/kyr) is in agreement with that of Zhao et al., (2017) for the LGM. In the Holocene, our modeled average accumulation rates are higher—UCC at approximately 9 g/cm<sup>2</sup>/kyr, 12 g/cm<sup>2</sup>/kyr for Luochuan, and 21 g/cm<sup>2</sup>/kyr total average accumulation—which coincides with a change in grain size from clay to silt and an increase in mean grain size (Figure 5) (Zhao et al., 2017). The coincident increases in SiO<sub>2</sub>/Al<sub>2</sub>O<sub>3</sub> and UCC may indicate very fine grained turbidites. Differences in grain size often indicate changes in distance between source and deposition location that may not be reflected by the overall chemistry. The strong agreement between these two independent data sets using widely different methods to determine provenance gives increased confidence in our understanding of the system. Additional discussion of grain size is continued in section 6.3.

During the LGM, the median accumulation rate of loess on the Chinese Plateau was 31 g/cm<sup>2</sup>/kyr (Kohfeld & Harrison, 2003), and fluxes are expected to decrease with distance from this depositional region. In comparison, the accumulation rates of the modelled Luochuan and Xiashu Loesses at Sites U1428 and U1429 reach 17 g/cm<sup>2</sup>/kyr accumulation rates during the LGM. The values of ~ 31 and 17 g/cm<sup>2</sup>/kyr are neither distinct enough from each other, nor close enough to each other, to make any substantive conclusion as to whether the loess material found in the sediment is air-borne or eroded from terrestrial deposits. Additional information is needed.

In this context, therefore, another approach is to compare the accumulation of the Luochuan and Xiashu loess-like end-members to present-day dust fluxes to the region, and compare to estimations of glacial dust fluxes. For example, Osada et al. (2014) measured present-day dry and wet dust deposition across Japan and estimated that modern dust deposition accumulates at rates of 0.4 to 1.2 g/cm<sup>2</sup>/kyr. If we assume that dust fluxes increased from two to four times the present fluxes during glacial periods (Hovan et al., 1989; McGee et al., 2010), reasonable glacial dust deposition estimates would result in accumulation rates of ~1 to 5 g/cm<sup>2</sup>/kyr. Given these estimates, therefore, the accumulation rate of the Luochuan Loess end-member at Sites U1428 and U1429 (15–23 g/cm<sup>2</sup>/kyr) is likely too large to be explained by purely eolian deposition, and at least a significant portion of it may be fluvially transported from the Asian interior. However, the accumulation of Xiashu Loess is consistent with this estimate, reaching maximum accumulation rates of 4–5 g/cm<sup>2</sup>/kyr at several glacial transition periods (Figure 6). Recall further that the Xiashu Loess end-member is a relatively small fraction of the total terrigenous supply, consistent with a recent independent study at this site (Zhao et al., 2017). The relatively small contribution of eolian material to the overall terrigenous accumulation at this site highlights the high potential for inadvertently confusing transport mechanisms for compositionally different sources despite similar assumptions of their own loess-like provenance.

### 6.3. Sea Level and Sediment Shelf Bypass

Pleistocene glacial cyclicity had a strong influence on sea level in the epicontinental seas of Asia (Berné et al., 2002; Saito et al., 1998; Yoo et al., 2016). Global reconstructions of sea level during the Pleistocene indicate sea level decreased as much as –130 m relative to present sea level (RSL) during glacial periods, and possibly rose to +20 m RSL during interglacials (Spratt & Lisiecki, 2016). The transgressions and regressions of the paleo-sea level influenced sediment delivery to deep marine systems and may be recorded as variability in sediment flux into the Okinawa Trough (Dou et al., 2010; Saito et al., 1998; Yoo et al., 2016).

While the local systematics are complex, the highstands, marked by increasing sea level, trap sediment closer to the mouths of rivers and along the Asian continental shelf. During these times, while the sediment accommodation space is large, a fine-grained sediment collects on the inner-continental shelf near the mouth of the Yangtze River (Xu et al., 2012) as well as in the Bohai Sea and Yellow Sea near the mouth of the Yellow River (Lim et al., 2006; Yoo et al., 2016). During glacial regressions, as sea level falls, the continental shelf is exposed and previously deposited sediment may be remobilized to deeper sediment systems as the paleo-shoreline recedes and river mouths advance.

Although the low-resolution nature of our current study precludes quantitative time series analysis, the records at Sites U1428 and U1429 document that the increases in total terrigenous flux in MIS 3 and MIS 6 precede minimum relative sea levels by several thousand years (Figure 6). This suggests that the potential remobilization of continental shelf sediment during glacial lowstands causes maximum sediment fluxes during the last stages of sea-level lowering rather than during the maximum lowstand itself. However, there is no discernable peak in terrigenous flux during MIS 8 or 10, other periods of lowest sea levels, which may indicate that multiple processes work in concert during the periods of the highest accumulation rates, or that the system is currently in transition from one mode to another.

Furthermore, changes in shelf exposure related to sea level is consistent with advancement of the Yellow and Yangtze rivers across the continental shelf toward the Okinawa Trough during glacial periods (Diekmann et al., 2008; Dou et al., 2016; Oiwan et al., 2011). The advancement of these major river mouths would predominantly focus sediment supply from the paleo-Yellow River to the region of Sites U1428 and U1429 in the Okinawa Trough, compared to the present when the sediment is trapped on the inner continental shelf (Xu et al., 2012). This transport mechanism may be indicated by the cyclicity in UCC and Luochuan Loess end-member accumulation rates, representing continental material (and in particular terrestrial deposits of loess) transported by the Yellow River directly supplying sediment. The peaks in UCC and Luochuan accumulation rates during interglacial periods (e.g., 65–80 kyr, 100–115 kyr, 175–185 kyr, and 290–320 kyr) may indicate increased riverine flux, while sea levels were still relatively low compared to present (Figure 6).

Exposure of the Bohai, Yellow, and East China Sea continental shelves would also facilitate remobilization of material through changes in the paleo-shoreline or eolian processes as sea level decreased during glacial periods. Reworking of these shelf deposits may cause increased accumulation rates of UCC and Luochuan Loess during times of sea level change. It would, however, take several thousand years for the river mouths to advance toward the shelf-break, and may increase the relative fraction of local material supply from the

Southern Japanese Islands to these sites. We hypothesize that the maximum rate of sediment deposition at this site is a reflection of maximum shelf exposure rate (as distinct from shelf exposure amount). As the continental shelf is newly exposed during periods of lower sea level, the maximum loss of shelf material reflects the maximum rate of shelf exposure, and therefore the highest accumulation rates in this depositional system.

Small peaks (2–7 g/cm<sup>2</sup>/kyr) occur in the Southern Japanese Islands end-member during coincident times of decreased UCC and Luochuan end-member accumulation and increased relative sea level. This is also mirrored in the LGM average Kyushu end-member accumulation rate identified by Zhao et al. (2017). Similar patterns of increased Southern Japanese Islands end-member accumulation and the grain size proxy SiO<sub>2</sub>/Al<sub>2</sub>O<sub>3</sub> (g/g) occur when relative sea level is also increased (Figure 5). This may reflect a shift to more localized sediment delivery of larger grain size (silts) from the Kyushu and the Japanese Archipelago, or fine-grained turbidites. It is, however, difficult to discern sediment remobilized from the exposed shelf versus sediment transported from terrestrial systems under shifting atmospheric and riverine conditions given our low temporal resolution.

The weathering signal may also be tied to changes in the hydrologic cycle in the Asian interior. Reconstructions of the Asian hydrologic cycle have focused on speleothems and paleosalinity records, in order to probe variability in the Asian Monsoon system and therefore precipitation and riverine flux (Clemens et al., 2010; Kubota et al., 2010). Chinese speleothem  $\delta^{18}\text{O}$  records (e.g., Cheng et al., 2016) show clear precessional variability and are interpreted as reflecting higher monsoon intensity during the precessional maxima in local summer insolation. Planktonic  $\delta^{18}\text{O}$  records from the South China Sea, possibly reflecting input from the Pearl River, also show precessional variability over the last 350 kyr (Caballero-Gill et al., 2012). It is unclear whether speleothem  $\delta^{18}\text{O}$  records reflect local precipitation compared to upstream monsoon precipitation. Similarly, the planktonic  $\delta^{18}\text{O}$  records may reflect changes in the  $\delta^{18}\text{O}$  of river end-members rather than in changes in volume of river inputs. If these records do reflect local precipitation, one would predict higher fluvial outflow and sediment flux during precessional maxima. Due to coarse temporal resolution, our sediment records do not exhibit clear precessional variability in terrigenous flux, which limit direct comparison to the aforementioned speleothem records. Additional on-going work by our research group on high-resolution XRF-scanning data may provide further information about this topic.

Given the body of previous research to investigate terrestrial and marine components recording the history of the Asian Monsoon, large-scale climate processes may not be interpreted in a direct or straight forward manner from similar, fluvial dominated sediments. Even with the low resolution record, it is clear that there are limited glacial-interglacial climate signals in the terrigenous provenance at these sites that likely indicate larger more complicated problems in reconstructions from fluvial sediments: influence from sea level change and shelf storage, as well as global climate processes and localized monsoonal variability. These processes also influence other fluvial deposition systems, so careful consideration is necessary to untangle specific, localized climate history from fluvial deposits.

## 7. Summary and Conclusions

We analyzed major, trace and rare earth elements in 82 bulk sediment samples from IODP Sites U1428 and U1429 in the East China Sea. We used multivariate statistical partitioning techniques to identify and quantify five sediment source components in these samples. Via CLS modeling, our results indicate that UCC, Luochuan Loess, Xiashu Loess, Southern Japanese Islands, and Kyushu Volcanics components are the end-members contributing aluminosilicate material to the East China Sea. The statistical identification of these end-members does not prescribe transportation mechanism, but interpretation is possible with other environmental records.

The physical changes to the local depositional environment through sea level, fluvial supply, eolian inputs, shelf-bypass, and volcanic processes all likely combined to different degrees through time to influence the record of terrigenous supply to Sites U1428 and U1429 during the last ~400 kyr. Mass accumulation rates of UCC and Luochuan Loess may reflect increased fluvial supply and reworking of loess-like material to these sites. The grain size proxy SiO<sub>2</sub>/Al<sub>2</sub>O<sub>3</sub> suggests several periods of increased grain size during intervals of increased sea level or rapid changes in climate, which may indicate increased supply of localized, larger grained sediment from the Japanese Islands. The Kyushu Volcanic end-member, while low in abundance, may record several well-characterized eruptions of the Aso Volcano or other compositionally similar volcanoes from the region. Higher-resolution studies via XRF in this region are necessary to answer key additional

climate questions related to shorter lived changes in the processes influencing atmospheric and hydrologic cycles in East Asia as related to the East Asian Monsoon.

#### Acknowledgments

We thank Mitch Lyle and one anonymous reviewer for the suggestions to improve the manuscript. We also express our appreciation to Shiming Wan for constructive conversations pertaining to these sites and his own on-going research. We also thank T. Ireland for analytical assistance at Boston University and greatly appreciate the lab assistance by A. Braunthal, and E. Sonshine. This research used samples and data provided by the Integrated Ocean Drilling Program (IODP). Funding for this research was provided by the U.S. National Science Foundation to R.W.M. (NSF-EAR1434175), L.G. (NSF-EAR1433665) and D.M. (NSF-EAR1434138). USSSP postcruise support was provided to Expedition 346 shipboard participants R.W.M., A.G.D., L.G., C.W.K., and R.T. Portions of this material are based upon work supported while R.W.M. was serving at the National Science Foundation. The data generated and used in this study are included in the supporting information.

#### References

- Berné, S., Vagner, P., Guichard, F., Lericolais, G., Liu, Z., Trentesaux, A., et al. (2002). Pleistocene forced regressions and tidal sand ridges in the East China Sea. *Marine Geology*, *188*, 293–315. [https://doi.org/10.1016/S0025-3227\(02\)00446-2](https://doi.org/10.1016/S0025-3227(02)00446-2)
- Caballero-Gill, R. P., Clemens, S. C., & Prell, W. L. (2012). Direct correlation of Chinese speleothem 18O and South China Sea planktonic 18O: Transferring a speleothem chronology to the benthic marine chronology. *Paleoceanography*, *27*, PA2203. <https://doi.org/10.1029/2011PA002268>
- Calvert, S. E., & Pedersen, T. F. (1993). Geochemistry of recent oxic and anoxic marine sediments: Implications for the geological record. *Marine Geology*, *113*, 67–88. [https://doi.org/10.1016/0025-3227\(93\)90150-T](https://doi.org/10.1016/0025-3227(93)90150-T)
- Chen, J., Hongtao, W., & Huayu, L. (1996). Behaviours of REE and other trace elements during pedological weathering: Evidence from chemical leaching of loess and palaeosol from the Luochuan section in Central China. *Acta Geologica Sinica*, *9*(3), 290–302. <https://doi.org/10.1111/j.1755-6724.1996.mp9003006>
- Chen, Y., Li, X., Han, Z., Yang, S., Wang, Y., & Yang, D. (2008). Chemical weathering intensity and element migration features of the Xiashu loess profile in Zhenjiang, Jiangsu province. *Journal of Geographical Sciences*, *18*, 341–352. <https://doi.org/10.1007/s11442-008-0341-9>
- Cheng, H., Edwards, R. L., Sinha, A., Spötl, C., Yi, L., Chen, S., et al. (2016). The Asian monsoon over the past 640,000 years and ice age terminations. *Nature*, *534*, 640–646. <https://doi.org/10.1038/nature18591>
- Clemens, S. C., Prell, W. L., & Sun, Y. (2010). Orbital-scale timing and mechanisms driving Late Pleistocene Indo-Asian summer monsoons: Reinterpreting cave speleothem D18O. *Paleoceanography*, *25*, PA4207. <https://doi.org/10.1029/2010PA001926>
- Clift, P. D., Wan, S., & Blusztajn, J. (2014). Reconstructing chemical weathering, physical erosion and monsoon intensity since 25Ma in the northern South China Sea: A review of competing proxies. *Earth-Science Reviews*, *130*, 86–102. <https://doi.org/10.1016/j.earscirev.2014.47201.002>
- Diekmann, B., Hofmann, J., Henrich, R., Fütterer, D. K., Röhl, U., & Wei, K. Y. (2008). Detrital sediment supply in the southern Okinawa Trough and its relation to sea-level and Kuroshio dynamics during the late Quaternary. *Marine Geology*, *255*, 83–95. <https://doi.org/10.1016/j.margeo.2008.08.001>
- Dou, Y., Yang, S., Liu, Z., Clift, P. D., Yu, H., Berne, S., et al. (2010). Clay mineral evolution in the central Okinawa Trough since 28 ka: Implications for sediment provenance and paleoenvironmental change. *Palaeogeography, Palaeoclimatology, Palaeoecology*, *288*, 108–117. <https://doi.org/10.1016/j.palaeo.2010.01.040>
- Dou, Y., Yang, S., Shi, X., Clift, P. D., Liu, S., Liu, J., et al. (2016). Provenance weathering and erosion records in southern Okinawa Trough sediments since 28 ka: Geochemical and Sr-Nd-Pb isotopic evidences. *Chemical Geology*, *425*, 93–109. <https://doi.org/10.1016/j.chemgeo.2016.01.029>
- Dunlea, A. G., & Murray, R. W. (2015). Optimization of end-members used in multiple linear regression geochemical mixing models. *Geochemistry, Geophysics, Geosystems*, *16*, 4021–4027. <https://doi.org/10.1002/2015GC006132>
- Dunlea, A. G., Murray, R. W., Sauvage, J., Spivack, A. J., Harris, R. N., & D'Hondt, S. (2015). Dust, volcanic ash, and the evolution of the South Pacific Gyre through the Cenozoic. *Paleoceanography*, *30*, 1078–1099. <https://doi.org/10.1002/2015PA002829>
- Expedition Scientists (Exp. 346) (2014). Onset and evolution of millennial-scale variability of Asian Monsoon and its possible relation with Himalaya and Tibetan Plateau uplift. *Integrated Ocean Drilling Program (IODP) Preliminary Report (1932-9423)*, 2014-09, N. 346. <https://doi.org/10.2204/iodp.proc.346.2015>
- Gale, A., Dalton, C. A., Langmuir, C. H., Su, Y., & Schilling, J. G. (2013). The mean composition of ocean ridge basalts. *Geochemistry, Geophysics, Geosystems*, *14*, 489–518. <https://doi.org/10.1029/2012GC004334>
- Gallagher, S., Kitamura, A., Iryu, Y., Itaki, T., Koizumi, I., & Hoiles, P. (2015). The Pliocene to recent history of the Kuroshio and Tsushima Currents: A multi-proxy approach. *Progress in Earth and Planetary Science*, *2*, 17. <https://doi.org/10.1186/s40645-015-0045-6>
- Gallet, S., Jahn, B.-M., & Torii, M. (1996). Geochemical characterization of the Luochuan loess-paleosol sequence, China, and paleoclimatic implications. *Chemical Geology*, *133*, 67–88. [https://doi.org/10.1016/S0009-2541\(96\)00070-8](https://doi.org/10.1016/S0009-2541(96)00070-8)
- Gao, S., Luo, T.-C., Zhang, B.-R., Zhang, H.-F., Han, Y.-W., Zhao, Zi-D., & Hu, Y.-K. (1998). Chemical composition of the continental crust as revealed by studies in East China. *Geochimica et Cosmochimica Acta*, *62*, 1959–1975. [https://doi.org/10.1016/S0016-7037\(98\)00121-5](https://doi.org/10.1016/S0016-7037(98)00121-5)
- Gong, Z., Chen, H., Wang, Z., Cai, F., & Luo, G. (1987). The epigenetic geochemical types of loess in China. In T. Liu (Ed.), *Aspects of loess research* (pp. 328–340). Beijing, China: China Ocean Press.
- Hao, Q., Guo, Z., Qiao, Y., Xu, B., & Oldfield, F. (2010). Geochemical evidence for the provenance of middle Pleistocene loess deposits in southern China. *Quaternary Science Reviews*, *29*, 3317–3326. <https://doi.org/10.1016/j.quascirev.2010.08.004>
- Hovan, S. A., Rea, D. K., Pisias, N. G., & Shackleton, N. J. (1989). A direct link between the China loess and marine [delta]18O records: Aeolian flux to the north Pacific. *Nature*, *340*, 296–298. <https://doi.org/10.1038/340296a0>
- Ikehara, K. (2015). Marine tephra in the Japan Sea sediments as a tool for paleoceanography and paleoclimatology. *Progress in Earth and Planetary Science*, *2*, 36. <https://doi.org/10.1186/s40645-015-0068-z>
- Ireland, T. J., Scudder, R. P., Dunlea, A. G., Anderson, C. H., & Murray, R. W. (2014). *Assessing the accuracy and precision of inorganic geochemical data produced through flux fusion and acid digestions: Multiple (60+) comprehensive analysis of BHVO-2 and the development of improved "Accepted" values*. Abstract V41A–4767 presented at 2014 Fall Meeting, Washington, DC: AGU.
- Irimo, T., & Tada, R. (2000). Quantification of Aeolian dust (Kosa) contribution to the Japan Sea sediments and its variation during the last 200 ky. *Geochemical Journal*, *34*, 59–93. <https://doi.org/10.2343/geochemj.34.59>
- Kawahata, H., Nohara, M., Aoki, K., Minoshima, K., & Gupta, L. P. (2006). Biogenic and abiogenic sedimentation in the northern East China Sea in response to sea-level change during the Late Pleistocene. *Global and Planetary Change*, *53*, 108–121. <https://doi.org/10.1016/j.gloplacha.2006.01.013>
- Kohfeld, K. E., & Harrison, S. P. (2003). Glacial-interglacial changes in dust deposition on the Chinese Loess Plateau. *Quaternary Science Reviews*, *22*, 1859–1878. [https://doi.org/10.1016/S0277-3791\(03\)00166-5](https://doi.org/10.1016/S0277-3791(03)00166-5)
- Kubota, Y., Kimoto, K., Tada, R., Oda, H., Yokoyama, Y., & Matsuzaki, H. (2010). Variations of East Asian summer monsoon since the last deglaciation based on Mg/Ca and oxygen isotope of planktic foraminifera in the northern East China Sea. *Paleoceanography*, *25*, PA4205. <https://doi.org/10.1029/2009PA001891>
- Lee, K. E., Lee, H. J., Park, J. H., Chang, Y. P., Ikehara, K., Itaki, T., et al. (2013). Stability of the Kuroshio path with respect to glacial sea level lowering. *Geophysical Research Letters*, *40*, 392–396. <https://doi.org/10.1002/grl.50102>

- Lim, D. I., Jung, H. S., Choi, J. Y., Yang, S., & Ahn, K. S. (2006). Geochemical compositions of river and shelf sediments in the Yellow Sea: Grain-size normalization and sediment provenance. *Continental Shelf Research*, 26, 15–24. <https://doi.org/10.1016/j.csr.2005.10.001>
- Lisiecki, L. E., & Raymo, M. E. (2005). A Pliocene-Pleistocene stack of 57 globally distributed benthic  $\delta^{18}O$  records. *Paleoceanography*, 20, PA1003. <https://doi.org/10.1029/2004PA001071>
- Liu, S., Shi, X., Fang, X., Dou, Y., Liu, Y., & Wang, X. (2014). Spatial and temporal distributions of clay minerals in mud deposits on the inner shelf of the East China Sea: Implications for paleoenvironmental changes in the Holocene. *Quaternary International*, 349, 270–279. <https://doi.org/10.1016/j.quaint.2014.07.016>
- Lu, H., & Guo, Z. (2013). Evolution of the monsoon and dry climate in East Asia during late Cenozoic: A review. *Science China Earth Sciences*, 57, 1–10. <https://doi.org/10.1007/s11430-013-4790-3>
- Martinez, N. C., Murray, R. W., Dickens, G. R., & Kölling, M. (2009). Discrimination of sources of terrigenous sediment deposited in the central Arctic Ocean through the Cenozoic. *Paleoceanography*, 24, PA1210. <https://doi.org/10.1029/2007PA001567>
- McGee, D., Broecker, W. S., & Winckler, G. (2010). Gustiness: The driver of glacial dustiness? *Quaternary Science Reviews*, 29, 2340–2350. <https://doi.org/10.1016/j.quascirev.2010.06.009>
- Morford, J. L., & Emerson, S. (1999). The geochemistry of redox sensitive trace metals in sediments. *Geochimica et Cosmochimica Acta*, 63, 1735–1750. [https://doi.org/10.1016/S0016-7037\(99\)00126-X](https://doi.org/10.1016/S0016-7037(99)00126-X)
- Nagashima, K., Tada, R., Tani, A., Toyoda, S., Sun, Y., & Isozaki, Y. (2007). Contribution of Aeolian dust in Japan Sea sediments estimated from ESR signal intensity and crystallinity of quartz. *Geochemistry, Geophysics, Geosystems*, 8, Q02Q04. <https://doi.org/10.1029/2006GC001364>
- Nagashima, K., Tada, R., & Toyoda, S. (2013). Westerly jet-East Asian summer monsoon connection during the Holocene. *Geochemistry, Geophysics, Geosystems*, 14, 5041–5053. <https://doi.org/10.1002/2013GC004931>
- Oiwane, H., Tonai, S., Kiyokawa, S., Nakamura, Y., Suganuma, Y., & Tokuyama, H. (2011). Geomorphological development of the Goto Submarine Canyon, northeastern East China Sea. *Marine Geology*, 288, 49–60. <https://doi.org/10.1016/j.margeo.2011.06.013>
- Osada, K., Ura, S., Kagawa, M., Mikami, M., Tanaka, T. Y., Matoba, S., et al. (2014). Wet and dry deposition of mineral dust particles in Japan: Factors related to temporal variation and spatial distribution. *Atmospheric Chemistry and Physics*, 14, 1107–1121. <https://doi.org/10.5194/acp-14-1107-2014>
- Pisias, N. G., Murray, R. W., & Scudder, R. P. (2013). Multivariate statistical analysis and partitioning of sedimentary geochemical data sets: General principles and specific MATLAB scripts. *Geochemistry, Geophysics, Geosystems*, 14, 4015–4020. <https://doi.org/10.1002/ggge.20247>
- Sagawa, T., Nagahashi, Y., Satoguchi, Y., Holbourn, A., Gallagher, S. J., Saavedra-Pellitero, M., et al. (2017). Integrated tephrostratigraphy and isotope stratigraphy in the Japan Sea and East China Sea using IODP sites U1427, U1426 and U1429, Expedition 346 Asian Monsoon. *Progress in Earth and Planetary Science*, 5, 18. <https://doi.org/10.1186/s40645-018-0168-7>
- Saito, Y., Katayama, H., Ikehara, K., Kato, Y., Matsumoto, E., Oguri, K., et al. (1998). Transgressive and highstand systems tracts and post-glacial transgression, the East China Sea. *Sedimentary Geology*, 122, 217–232. [https://doi.org/10.1016/S0037-0738\(98\)00107-9](https://doi.org/10.1016/S0037-0738(98)00107-9)
- Scudder, R. P., Murray, R. W., Schindlbeck, J. C., Kutterolf, S., Hauff, F., Underwood, M. B., et al. (2016). Geochemical approaches to the quantification of dispersed volcanic ash in marine sediment. *Progress in Earth and Planetary Science*, 3, 1. <https://doi.org/10.1186/s40645-015-0077-y>
- Spratt, R. M., & Lisiecki, L. E. (2016). A Late Pleistocene sea level stack. *Climate of the Past*, 12, 1079–1092. <https://doi.org/10.5194/cp-12-1079-2016>
- Tada, R. (2004). Onset and evolution of millennial-scale variability in the Asian monsoon and its impact on paleoceanography of the Japan Sea. In P. Clift et al. (Eds.), *Continent-ocean interactions within East Asian marginal seas* (Vol. 149, pp. 283–298). Washington, DC: American Geophysical Union. <https://doi.org/10.1029/GM15>
- Tada, R., Murray, R. W., & Alvarez Zarikian, C. A. (2013). Asian Monsoon: Onset and evolution of millennial-scale variability of Asian Monsoon and its possible relation with Himalaya and Tibetan Uplift. *Integrated Ocean Drilling Program (IODP) Scientific Prospectus 346*. <https://doi.org/10.2204/iodp.sp.346.2013>
- Taylor, S. R., & McLennan, S. M. (1985). *The continental crust: Its composition and evolution*. Palo Alto, CA: Blackwell Scientific.
- Taylor, S. R., McLennan, S. M., & McCulloch, M. T. (1983). Geochemistry of loess, continental crustal composition and crustal model ages. *Geochimica et Cosmochimica Acta*, 47, 1897–1905. [https://doi.org/10.1016/0016-7037\(83\)90206-5](https://doi.org/10.1016/0016-7037(83)90206-5)
- Uehara, K., Saito, Y., & Hori, K. (2002). Paleotidal regime in the Changjiang (Yangtze) Estuary, the East China Sea, and the Yellow Sea at 6 ka and 10 ka estimated from a numerical model. *Marine Geology*, 183, 179–192. [https://doi.org/10.1016/S0025-3227\(01\)00255-9](https://doi.org/10.1016/S0025-3227(01)00255-9)
- Ujiié, H., & Ujiié, Y. (1999). Late Quaternary course changes of the Kuroshio Current in the Ryukyu Arc region, northwestern Pacific Ocean. *Marine Micropaleontology*, 37, 23–40. [https://doi.org/10.1016/S0377-8398\(99\)00010-9](https://doi.org/10.1016/S0377-8398(99)00010-9)
- Wan, S., Li, A., Clift, P. D., & Stuut, J.-B. W. (2007). Development of the East Asian monsoon: Mineralogical and sedimentologic records in the northern South China Sea since 20 Ma. *Palaeogeography, Palaeoclimatology, Palaeoecology*, 254, 561–582. <https://doi.org/10.1016/j.palaeo.2007.07.009>
- Wang, P., Clemens, S., Beaufort, L., Braconnot, P., Ganssen, G., Jian, Z., et al. (2005). Evolution and variability of the Asian monsoon system: State of the art and outstanding issues. *Quaternary Science Reviews*, 24, 595–629. <https://doi.org/10.1016/j.quascirev.2004.10.002>
- Webster, P. J., Magaña, V. O., Palmer, T. N., Shukla, J., Tomas, R. A., Yanai, M., et al. (1998). Monsoons: Processes, predictability, and the prospects for prediction. *Journal of Geophysical Research*, 103, 14451–14510. <https://doi.org/10.1029/97JC02719>
- Xu, K., Li, A., Liu, J. P., Milliman, J. D., Yang, Z., Liu, C. S., et al. (2012). Provenance, structure, and formation of the mud wedge along inner continental shelf of the East China Sea: A synthesis of the Yangtze dispersal system. *Marine Geology*, 291–294, 176–191. <https://doi.org/10.1016/j.margeo.2011.06.003>
- Yoo, D. G., Lee, G. S., Kim, G. Y., Kang, N. K., Yi, B. Y., Kim, Y. J., et al. (2016). Seismic stratigraphy and depositional history of late Quaternary deposits in a tide-dominated setting: An example from the eastern Yellow Sea. *Marine and Petroleum Geology*, 73, 212–227. <https://doi.org/10.1016/j.marpetgeo.2016.03.005>
- Zhao, D., Wan, S., Toucanne, S., Clift, P. D., Tada, R., Revillon, S., et al. (2017). Distinct control mechanism of fine-grained sediments from Yellow River and Kyushu supply in the northern Okinawa Trough since the last glacial. *Geochemistry, Geophysics, Geosystems*, 18, 2949–2969. <https://doi.org/10.1002/2016GC006764>
- Zheng, H., Clift, P. D., Wang, P., Jia, J., He, M., & Jourdan, F. (2013). Pre-Miocene birth of the Yangtze River. *Proceedings of the National Academy of Sciences of the United States of America*, 110, 7556–7561.
- Ziegler, C. L., Murray, R. W., Hovan, S. A., & Rea, D. K. (2007). Resolving eolian, volcanogenic, and authigenic components in pelagic sediment from the Pacific Ocean. *Earth and Planetary Science Letters*, 254(3–4), 416–432. <https://doi.org/10.1016/j.epsl.2006.11.049>